A biomechanical model for cell sensing and cell migration

Ian Manifacier, Arnaud Chauvière, Claude Verdier, Grégory Chagnon, Ibrahim Cheddadi, Nicolas Langlade, Angélique Stéphanou

A biomechanical model for cell sensing and cell migration

Ian Manifacier[1], Arnaud Chauvière[1], Claude Verdier[2], Grégory Chagnon[1], Ibrahim Cheddadi[1], Nicolas Glade[1], and Angélique Stéphanou[*1]

[1]*Université Grenoble Alpes, CNRS, UMR 5525, VetAgro Sup, Grenoble INP, TIMC, 38000 Grenoble, France*

[2]*Université Grenoble Alpes, CNRS, UMR 5588, LIPhy/MC[2], 38000 Grenoble, France*

November 4, 2022

1 Introduction

A fascinating aspect of how cells interact to create multi-cellular structures is largely stochastic [1, 2]. The combined complexity and randomness involved in such processes makes it difficult to unravel the interwoven ingredients needed for various multi-cellular structures to emerge [3, 4]. However, for emergence to happen, each cell needs to behave in a sufficiently coherent manner [5]. Therefore by studying cells individually in a controlled environment we may hope to identify a few key ingredients. Although single cell migration is stochastic, it can nonetheless be influenced by the inherent properties of the substrate. Known examples include, cell to substrate adhesion properties [6], substrate stiffness [7], substrate topology [8] and the shape of the adhesion patterns drawn on the substrate [2].

The effect of adhesion properties on cell motility was reported in 1997 by Palecek *et al.* [6] and largely confirmed by other groups since then [9]. Interestingly, experiments showed that, as the mean detachment force increases, the mean cell speed would initially increase, then peaked and finally declined [6].

[*]angelique.stephanou@univ-grenoble-alpes.fr

On the other hand, directional migration bias can be observed in some instances when single cells are allowed to migrate between adhesion patterns. Vecchio *et al.* [2] reported a significant bias as single cells moved between triangular patterns coated with fibronectin [10]. Understanding how cells perceive and react to their surrounding should ultimately enable us to better comprehend how biological processes such as tissue formation and angiogenesis take place. We therefore chose to use a numerical model as a tool to test our hypothesis and the limits of our theoretical understanding.

Various types of numerical models can already be found in the literature. Each type has its own advantages and drawbacks. Lattice based models, such as Cellular Potts Models and cellular automata are defined on a grid, which artificially constraints the cell behavior, notably when it comes to accurately model the impact of mechanics in the system [11, 12, 13]. Others are point based models, which have the advantage of being simple, on the other hand, it means that no intracellular mechanics is taken into account and external mechanics is also limited [14]. Finally, more complex mechanical cellular models such as the one presented by [15, 16, 17] are numerically too costly and too complex, making them impracticable to study cellular migration and behavior on large scales.

We therefore developed an agent based cellular model with moderate complexity, making it computationally light and fast enough to run a moderately large number of simulation on a regular computer within a reasonable time frame, while being rich enough to take into account some aspect of the intracellular mechanics. The model is composed of nodes and branches. The nodes connect the branches to each other and can interact with the substrate, while the branches transmit and generate forces between nodes. This design allows for the emergence of a dynamic cellular structure. The behavior of the model was then tested on homogeneous substrates with various adhesion conditions so as to identify the key parameters needed to recreate the hump like curve found by [6] and by [9]. In addition, the model was also tested on triangular shape adhesion patterns to identify relevant parameters involved in directional biases [10], [2].

2 Cell model

2.1 Overall cell structure

Our cell model is constructed to account for the overall cell dynamics based on the interactions between cytoskeletal fibres and adhesion points. It is composed of branches and nodes that form a hierarchical tree like structure meant to represent the mechanical structure of the cell by emulating its center (nucleus), membrane protrusions, adhesions and mechanosensors. Each node N_i has an order i (from 1 to 2) that indicates its degree of separation from the central node N_0. The parent node of N_i is node N_{i-1}. Node N_0 has no parent node. Several N_i nodes can radiate from a node N_{i-1} and each branch B_i connects the two nodes N_i and N_{i-1}.

- The N_0 node represents the cell center, (*i.e.* the cell nucleus). This point is unique and it is used to locate the cell.
- The N_1 node represents a cell adhesion as the tip of a protrusion emanating from the cell centre. N_1 nodes have the potential to maturate and exist under three different forms of increased maturity (described below) in order to account for the evolving nature of the cell adhesions.
- The N_2 node represents a protruding mechanosensor. Those nodes typically represent membrane extensions, such as filopodia, that probe the cell environment.

The number, position and properties of nodes and branches are dynamically regulated, such that the cell generates or deletes nodes and branches. The latter transmit and generate forces thus enabling nodes to move and pull on the substrate. The cell can consequently spread, adhere, pull and move. The behavior of each node is dependent on its order, thus enabling the emergence of a coherent system. The rules regulating each node type are summarized in Figure 1 and are detailed below.

2.2 Nodes generation

N_1 nodes

Several N_1 nodes can be generated during the cell's life time. The frequency and the location at which they are generated is regulated in a probabilistic manner. Therefore, to determine how many N_1 nodes should be generated during the current time step, we first need to calculate the occurrence of independent events that will attempt to

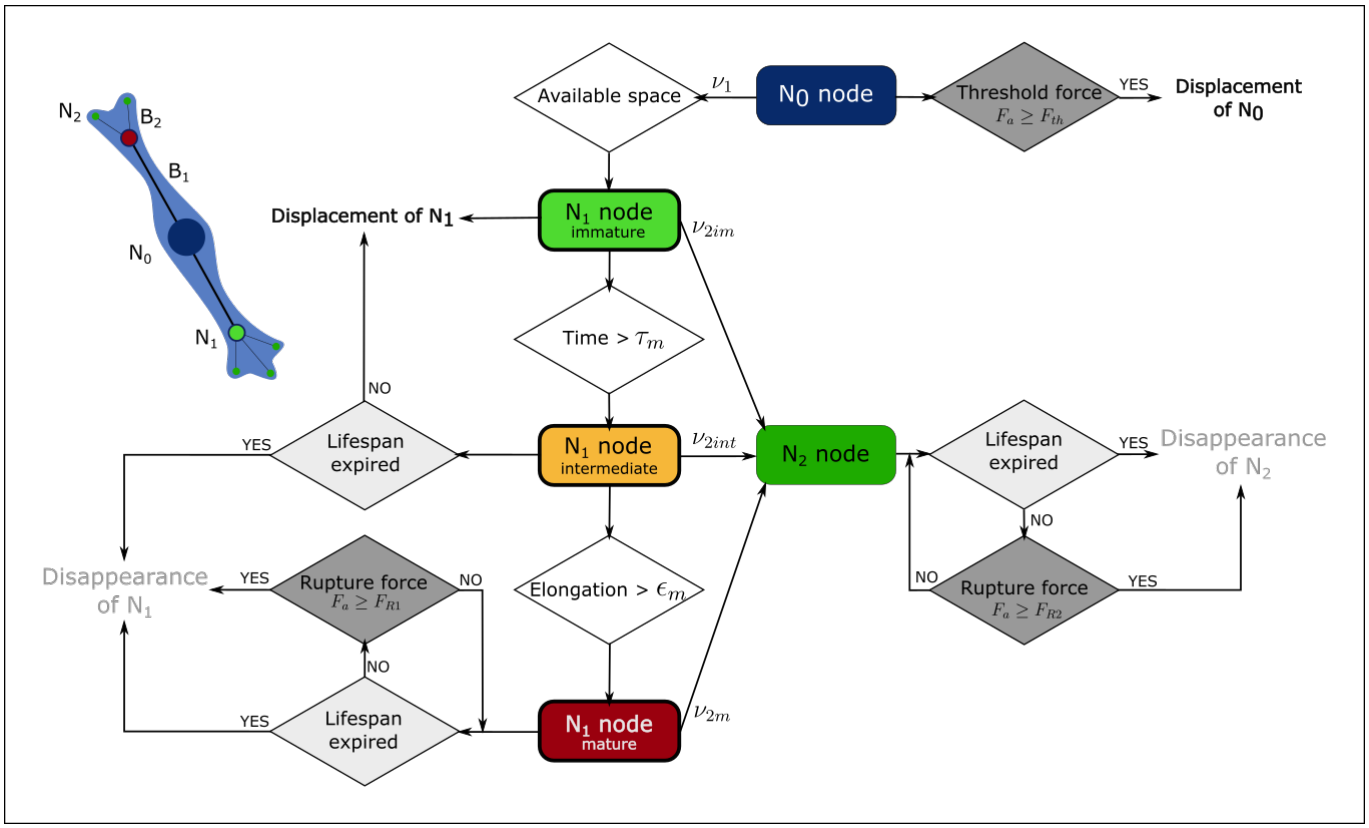

Figure 1: The cell structure is composed of nodes and branches, N_0, the root node is at the center, B_1 branches connect the root node to N_1 nodes and B_2 branches connect the latter to N_2 nodes. The flowchart shows how nodes evolve over time. The N_0 node is bound to the substrate and moves if the adhesion force F_a is greater than the threshold force F_{th}. It generates N_1 nodes if space is available. N_1 nodes are initially immature, then intermediate and finally mature. The respective function of each N_1 state is to: explore (if immature), assess if it can become mature (if intermediate) and bind to the substrate (if mature). During each maturation state a N_1 node respectively generates N_2 nodes at an average stochastic rate of ν_{2im}, ν_{2int} and ν_{2m}. The function of the N_2 nodes is to probe the environment and contribute to the movement of the cell's leading edge. Therefore, immature and intermediate N_1 nodes move, while mature N_1 nodes are bound to the substrate. Immature N_1 nodes transition to an intermediate state after reaching the age of τ_t, while the mature state is reached once the B_1 branch is strained above ε_m. When the adhesion force F_a of a N_1 or N_2 node is greater than the respective rupture force F_{R1}, F_{R2} there is rupture and the node disappears and its child nodes with it.

generate them. To do so, we define the mean frequency ν_1 at which these independent events occur around the cell. But, to avoid overcrowding of N_1 nodes in one area, an exclusion angle $\delta\theta_1$ is defined around the B_1 branch, so as to prevent new N_1 nodes from forming too close to their already existing counterparts (Fig. 2). From there we can then calculate λ_1, the expected rate of occurrence during a time step dt:

$$\lambda_1 = \nu_1 dt \tag{1}$$

Then we use a pseudo-random variate generator that follows the Poisson's distribution with λ_1 as input. The obtained random variate integer j_1 is the number of events that will attempt to create a N_1 node during the current time step. If j_1 is greater than zero and if there is room to create a new node, then a new node is created at a fixed initial distance l_{10} from N_0 and at a randomly generated angle θ_1 (fig. **??**). Where the latter is a random variate pulled from a uniform distribution over the angular domain that remains available. This process is repeated j_1 times or until there is no more room to create another node because the angular domain is fully inhibited.

N_2 nodes

N_2 nodes can be considered as membrane spikes that probe the cell environment. N_2 nodes are stochastically emitted by the parent N_1 node with a mean frequency ν_2 that depends on the maturation level of N_1. An immature N_1 emits N_2 nodes with a higher frequency to actively probe the environment and orient the cell displacement. As it maturates, the N_1 node reinforces its adhesion strength to the substrate and emits N_2 nodes with a lower frequency to progressively reduce the probing activity and stabilize the adhesion. The expected rate of occurrence λ_2 of a new N_2, during a time step dt, is:

$$\lambda_2 = \nu_2 dt \tag{2}$$

a Poisson's variate generator is used to define the number of N_2 nodes that are created during the time step with λ_2 as input. Then the angle with which each new N_2 appears, is defined using a uniform-random variate generator that follows a uniform distribution. The sample space is defined between $\theta_1 \pm \delta\theta_2$. The new N_2 node is thus created at the angle θ_2 and fixed at an initial distance l_{20} from the position of the parent N_1 node (Fig. 2).

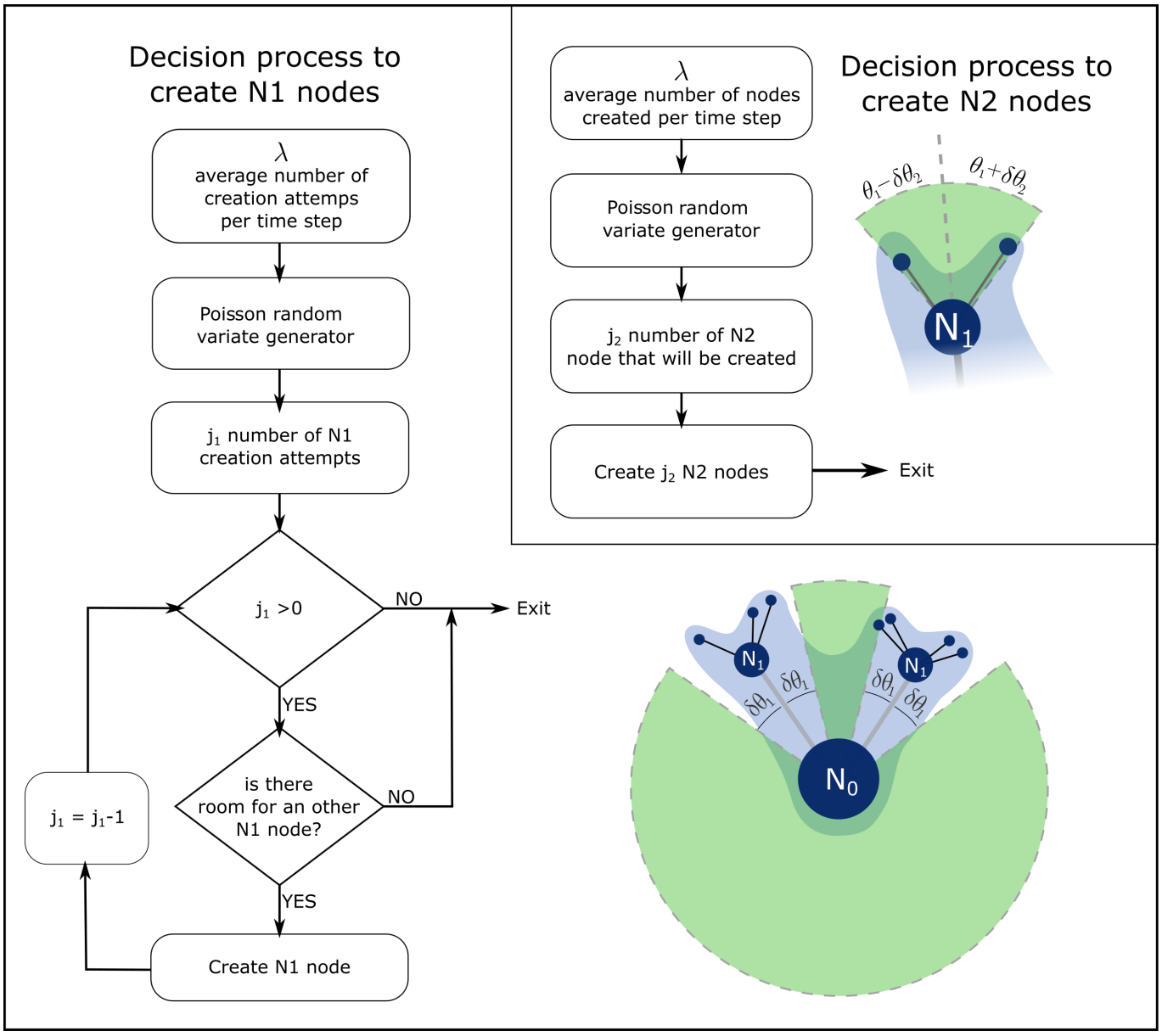

Figure 2: Nodes creation. *Left and bottom:* decision process to create N_1 nodes at each time step. A N_1 node located at an angle θ_1 will inhibit the formation of new N_1 nodes in the angular domain surrounding the B_1 branch *i.e.* $\theta_1 \pm \delta\theta_1$. *Top right:* Decision process to create N_2 nodes at each time step in an angular domain surrounding the B_1 branch *i.e.* $\theta_2 \pm \delta\theta_2$. Areas in green represents the zone where a new node can be created.

2.3 Nodes displacement

Our model aims at describing the cell movement and displacement dynamics. Therefore the nodes that all adhere to the substrate with various degrees, that depend on their type and maturation level, can be displaced by the mechanical forces applied on them through the branches.

Each branch (of index i) that is connected to a node exerts a force $\mathbf{F}_i$ on the node such that the net force applied by the n branches on the node is the sum of these forces. If the node is bound to the substrate the adhesion force $\mathbf{F}_a$ prevents the node from moving such that:

$$\mathbf{F}_a = -\sum_{i=1}^{n} \mathbf{F}_i \tag{3}$$

On the other hand, when the node is able to move, according to the quasi-static approximation the acceleration is negligible. Thus using Newton's second law, and by stating that the friction force $\mathbf{F}_v = -\alpha\mathbf{v}$ is always opposed to the node's displacement with velocity $\mathbf{v}$, we have:

$$-\alpha\mathbf{v} = \sum_{i=1}^{n} \mathbf{F}_i \tag{4}$$

where α is the friction coefficient of the node with the substrate. It depends on the node type and maturation level. The node's new position at the next iteration noted $\mathbf{x}_N^{t+dt}$ is thus given by:

$$\mathbf{x}_N^{t+dt} = \mathbf{x}_N^t + \mathbf{v}dt \quad \text{with} \quad \mathbf{v} = \frac{1}{\alpha}\sum_{i=1}^{n} \mathbf{F}_i \tag{5}$$

In our model, N_2 nodes play the role of sensors that interact with the substrate to probe its mechanical and/or adhesive properties in order to orientate the cell displacements. Several N_2 nodes are simultaneously linked by B_2 branches to their parent node N_1 on which they pull. B_2 branches are assumed to be short elastic actin spikes with elastic coefficient κ_2. They are emitted with an initial length l_{20} and they are characterized by a predefined Cauchy strain ε_{20} such that the resting length l_{2r} of the spike is smaller than its initial length, *i.e.* :

$$\varepsilon_{20} = \frac{l_{20} - l_{2r}}{l_{2r}} > 0 \tag{6}$$

As a consequence the spike is initially stretched and will attempt to return to its rest length. This will cause the branch to pull on both nodes, giving rise to a positive elastic force F_{el} along the $\overrightarrow{N_1N_2}$ axis since the N_2 node is fixed (bounded to the substrate) and the N_1 node is free to move (at least in its non mature states):

$$F_{el} = max(0, \kappa_2(l_2(t) - l_{2r})) \quad \text{with} \quad l_{2r} = \frac{l_{20}}{1+\varepsilon_{20}} \tag{7}$$

The resulting force on the parent node N_1 is calculated as the sum of the elastic contributions of each B_2 branches with equation (4). The N_1 node is then displaced according to equation (5) to its new position which corresponds to the location where the highest resulting tension is developed.

2.4 Nodes maturation

The N_1 nodes represent the adhesion points on which the cell actin fibres, represented by the B_1 branches, take support. Before the cell is able to move, the adhesion initially composed of integrins, should reinforce by the recruitment of new proteins such as talin and paxillin. Further proteins are recruited for the nucleation and binding of actin fibres, including vinculin, α-actinin, FAK, VASP, Arp2/3. The fibres can then generate increasing forces on the adhesion that reaches maturation under the form of a focal adhesion through the recruitment of zyxin and tensin. Reciprocally the mature adhesions can resist higher tensions from the cytoskeletal fibres. This bi-directional maturation process between adhesion and cytoskeletal fibres is important to realistically describe the cell sensing ability and its evolving biomechanics. Indeed, depending on the mechanical nature (rigidity) of the substrate the maturation process will be more or less efficient depending on the level of forces attained by the cell fibres.

We consider in the model three level of maturation for the N_1 nodes and its associated B_1 branch: immature, intermediate and mature states. Each state is characterized by an enhanced adhesiveness to the substrate and by an enhanced potential of force generation (Fig. 3).

- *Immature state:* the N_1 node is free to move and is displaced by the forces exerted by the N_2 nodes emitted at a high rate ν_{2im}. Consequently its friction with the substrate is initially small with coefficient α_{01} and linearly increases with time to reach at time τ_t the value α_{int} which characterizes the friction of the intermediate state. The friction evolution between the immature and intermediate states is thus given by:

$$\alpha_1(t) = \frac{\alpha_{int} - \alpha_{10}}{\tau_t}\, t + \alpha_{10} \tag{8}$$

As a concomitant event, the B_1 branch is progressively reinforced by actin fibres recruitment, that leads to a

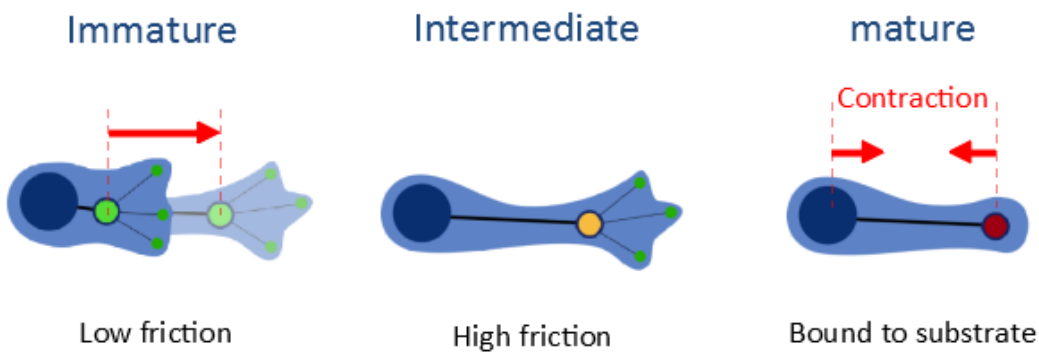

Figure 3: Illustration of the maturation stages of the $N1$ node. The immature node, characterized by a low friction with the substrate, is displaced by the traction of the N_2 nodes. After some pre-defined time the N_1 node reaches the intermediate maturation state characterized by an increased friction with the substrate. It finally reaches maturation if the B_1 branch is sufficiently elongated by the tensions from the N_2 nodes. The mature adhesion is bounded to the substrate and the B_1 branch becomes contractile to generate higher forces on the N_0 node in order to allow the cell to translocate by taking support on the N_1 node to move forward.

linearly increasing stiffness from κ_{10} (immature state) to κ_{11} (intermediate state):

$$\kappa_1(t) = \frac{\kappa_{11} - \kappa_{10}}{\tau_t} t + \kappa_{10} \tag{9}$$

The branch initially corresponds to an unstretched spring of length l_{01} that can bear tension and compression depending on the node displacement $l_1(t)$. The elastic restoring force in the branch is then given by:

$$F_{el} = \kappa_1(t)(l_1(t) - l_{01}) \tag{10}$$

- *Intermediate state:* it is attained when the N_1 node reaches the age τ_t for which the values of the friction coefficient and branch stiffness are kept constant as:

$$\alpha_1(t) = \alpha_{int} \quad \text{and} \quad \kappa_1(t) = \kappa_{11} \tag{11}$$

The increased friction coefficient of the node N_1 makes it resist more to the displacement from the pulling N_2 nodes. Moreover, the production rate of N_2 nodes is concomitantly reduced with $\nu_{2int} < \nu_{2im}$. This reduces significantly the exploration potential of the branch. At this stage, the B_1 branch corresponds to a bundle of actin fibres for which the rest length is reassessed and given by $l_1(\tau_t)$. The elastic restoring force in the branch

is now given by:

$$F_{el} = \kappa_{11}(l_1(t) - l_1(\tau_t)) \tag{12}$$

- *Mature state:* the transition to this state only occurs if the B_1 branch elongation from its new resting length $l_1(\tau_t)$ reaches the elongation target ε_m, *i.e.* if:

$$\frac{l_1(t) - l_1(\tau_t)}{l_1(\tau_t)} \geq \varepsilon_m \tag{13}$$

This condition is not necessarily reached, so not all N_1 maturate to this final state. If they do, two major transitions affect the node and branch. First, the node is fixed, bound to the substrate, in order to be able to sustain cell translocation that is required for the cell displacement. The production rate of N_2 is further reduced with $\nu_{2m} < \nu_{2int}$. Second, the branch becomes contractile, through myosin recruitment, and corresponds to a stress fibre which is able to generate the force required for the cell translocation, *i.e.* the force that will allow the N_0 node to move. The contractile force is given by:

$$F_c = \gamma_{max}(1 - e^{-\frac{\|\mathbf{F}_a\|}{F_\gamma}}) \tag{14}$$

where γ_{max} is the stall force of the adhesion, F_γ is a characteristic force constant, and $\|\mathbf{F}_a\|$ is the norm of the adhesion force. By convention, if $\mathbf{F_c}$ is positive, it pulls on N_0 whereas it pushes when it is negative. The total force in the branch is the sum of the elastic contribution F_{el} (Eq. (12)) and contractile one F_c (Eq. (14)). The cell translocation occurs if the adhesion force F_a (Eq. (3)) is bigger than a threshold force F_{th}.

2.5 Nodes disappearance

Nodes can disappear in two different ways. First they have a limited lifespan and they spontaneously disappear when this time limit is reached. The lifespan depends on the node type (see Table 1). Second the nodes that are bound to the substrate can be broken if the resulting tension force exerted on the node exceed the rupture force. In both cases, when the node disappears, the connecting branch and child nodes also disappear instantaneously.

3 Results

3.1 General cell behavior

The model aims at genericity, *i.e.* at representing potentially any cell types. A particular cell type can be generated by adjusting the parameters in order to obtain a specific cell shape (from round shape to stellar shape) and specific behavior defined by the cell motile potential for example. Cells as different as keratocytes and glial cells can be generated. For the simulations presented here, the model parameters (given in Table 1) were defined based on a set of predefined constraints to represent an average unspecified cell, as follows:

1. *cell shape:* the observation of isolated cells in two-dimensional cell culture shows that the cell shapes usually exhibit a limited number of main protrusions, rarely exceeding 4 branches (endothelial cells [ref] or fibroblasts [ref]). We fixed this limit as a first constraint with the parameter $\delta\theta_1$. The ability to form membrane spikes to probe the environment is in the other hand defined by the parameter $\delta\theta_2$.

2. *cell size:* the branches length l_{01} and l_{02}, used to define B_1 and B_2, were set to correspond to a protrusion and spike lengths respectively so that the maximum size of the cell does not exceed $50\mu m$ to remain within the values of an average cell size.

3. *cell force generation:* the cell mechanical properties defined by the cell stiffness coefficients (κ) and adhesion coefficients (α) were set so that the cell can develop the required range of forces, typically around $50nN$. The progressive increased in force generation associated to the maturation of the adhesions and fibres is obtained by making these parameters evolve along the 3 maturation states.

4. *cell motile dynamics:* time parameters such as adhesions production rates (ν) and adhesion lifespans (τ) contribute to the dynamics of the cell. But more importantly, the adhesions rupture forces (F_R) and the threshold force required for cell translocation (F_{th}) determine the level of interaction of the cell with its substrate and its ability to easily detach in order to move.

A suitable set of parameters that responds to these constraints and to the admissible range of values from the literature has been semi-empirically determined (see Table 1). The simulation realized with the so-defined parameters is presented in figure 4.

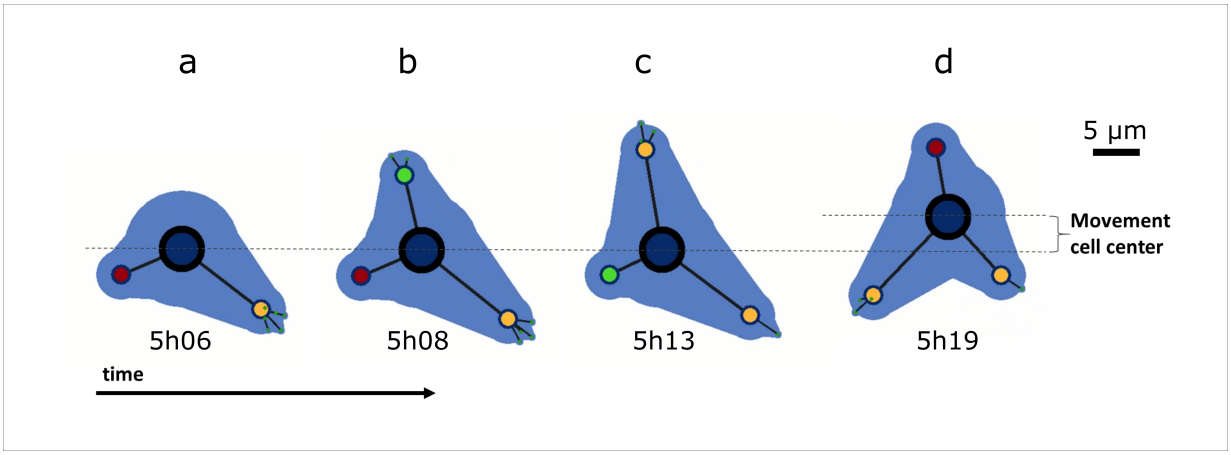

Figure 4: Cell deformation and migration observed over a 13 minutes period of a long lasting simulation of 72 hours. The cell mainly exhibits a characteristic triangular shape, with dynamical movements of extension/retraction of its protrusions (branches). Colour code for N_1 node states: green for immature, yellow for intermediate and red for mature. The cell envelop in blue is represented for cosmetic purpose only, since this model does not describe the cell membrane nor the cytoplasm.

Figure 4 shows a typical sequence of cell shape changes, in relation to the maturation of the nodes, and leading to the cell displacement. The simulation exhibits three different outcomes for the N_1 nodes: (i) a mature node disappears and is instantaneously replaced by an immature node (node on the left of the cell), (ii) a node is displaced, but the branch is not sufficiently elongated to reach the maturation criterion (node on the right of the cell), (iii) a node progressively and successfully evolves through the three maturation stages and eventually the contraction of the mature branch leads to the cell displacement (node on the top of the cell).

Adhesions dynamics

Cell deformations and migration have been simulated over 72 hours. The different events related to the nodes dynamics, including maturation and turnover, have been recorded. Figure 5a shows the cause of the N_1 nodes disappearance: among the 642 N_1 nodes generated, 366 (57%) disappear at the intermediate stage as their lifespan expired and 273 (43%) reach the mature state. Only 20% of the mature N_1 nodes attain their time limit, all the other mature nodes break because of the tensions forces applied on them. This relatively high contribution of the rupture force reveals that only a limited amount of mature adhesions N_1, are strong enough to resist the branch contractility as focal adhesions would. If the adhesion is strong enough to support cell translocation the cell will move, if it is not strong enough the adhesion breaks (rupture). On the other hand, the main cause of death of the 8815 generated N_2 nodes is the expiration of their lifespan that accounts for 82% of the disappearances (Fig. 5b). Indeed, the role of N_2 nodes is to dynamically

probe the environment. Their lifespan has been fixed short enough to favour this rapid dynamics, but long enough for the B_2 branches to exert tension forces to relocate the N_1 node in the region of interest (in the case of a heterogeneous substrate).

The maturation dynamics of the N_1 node is highlighted in figures 5c and 5d. All the 642 N_1 nodes formed during the 72 hour simulation maturate to the intermediate state since this transition is unconditional as soon as the node is 300 seconds old. At the intermediate state, the lifespan of the N_1 nodes is around 900 seconds. However if the branch B_1 elongates sufficiently, the node maturates and this can occur over a vast period of time (as shown in fig 5d) with an average time of $233 \pm 139s$, *i.e.* well before reaching the lifespan limit. This ensures that a sufficient amount (about 43%) of N_1 nodes will maturate. Once maturation is reached, an enhanced force competition - with the addition of a contractile force component - takes place in the branch. Rupture of the N_1 nodes occurs on a relatively short window period of $95 \pm 96s$ after the node reaches maturation. The remaining nodes reach their time limit of about 2000 seconds.

Force generation

Adhesions and branches maturate concomitantly. The maturation of the branch is characterized by the progressive increase of the force it can generate on its nodes. Figure 6 displays the evolution of the forces generated in the branches and exerted on the nodes during a sequence of a single cell movements of about one hour in order to highlight how the forces in the branches drive the nodes displacement dynamics and the cell migration. Figure 6, upper graph shows that at the immature stage, the forces in the B_1 branches remain very small despite the linear increase of the elasticity coefficient with time. After 300s the elasitcity coefficient of the branch stops evolving and the branch resting length is redefined to its acquired length. These new conditions define the intermediate state of the branch where the force progressively increases, often above 20nN, because of the branch elongation due to the N_1 node displacement under the traction of the B_2 branches (not represented). If the B_1 branch elongation reaches the elongation threshold ε_m then the B_1 branch attains the mature state and becomes contractile. This acquired contractility generates a jump of about 40nN in the branch force. This value has been defined so as to generate a level of force on N_0 sufficiently high to displace this node, *i.e.* for the cell to migrate. Figure 6, lower graph shows the resulting forces applied by the branches on the nodes. Forces applied on the N_1 nodes appear as a succession of spikes of about 20nN in intensity. This spike profile is explained by the N_1 node displacement that dissipate the resulting force from the B_1 and B_2 branches. Force

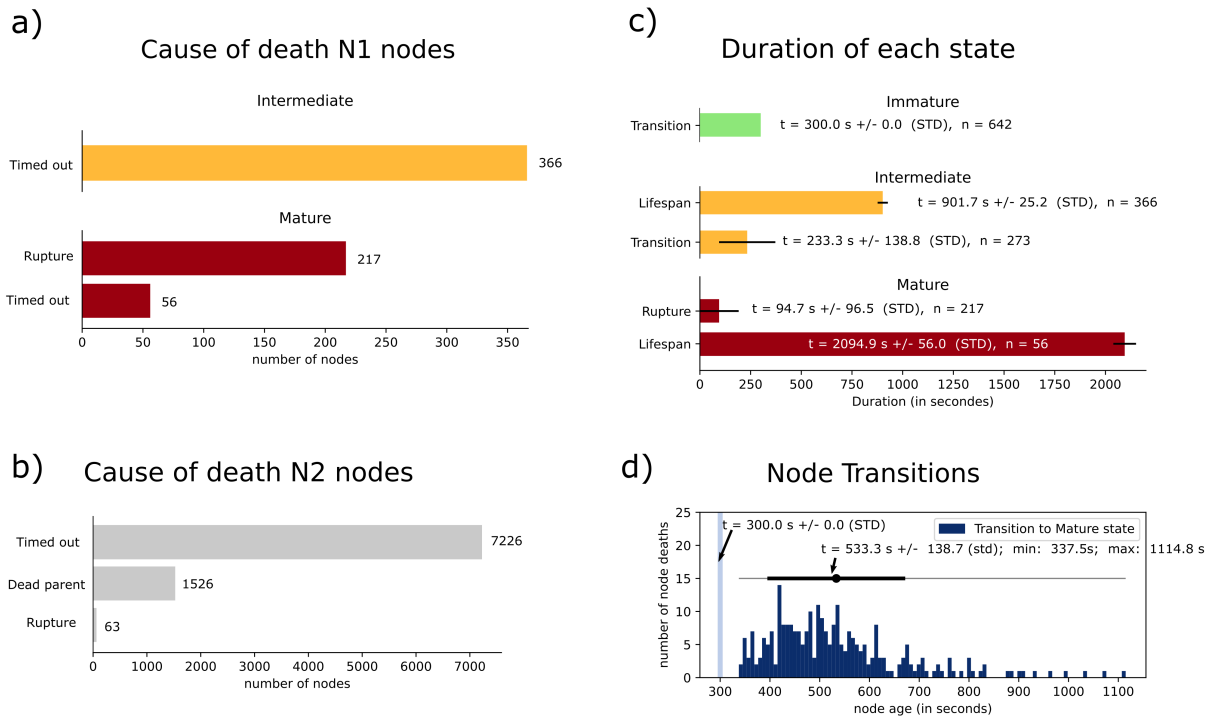

Figure 5: Nodes dynamics for a single cell over a 72 hour simulation. a) cause of death for the intermediate and mature N_1 nodes; b) cause of death of the N_2 nodes; c) durations at which the transitions to the more mature states occur, effective durations of the nodes lifespan and mean duration at which a mature node breaks (STD stands for standard deviation of the mean); d) recorded N_1 node transition events in function of the node age. All immature to intermediate transitions happened at the age of 300s, while all intermediate to mature transitions happened afterwards. The horizontal grey line spans from the earliest to the latest transition, while the black spot and bar show mean transition age and its standard deviation. We note that the node age is the sum of the times spent in each state. Colour code for N_1 node states: green for immature, yellow for intermediate and red for mature.

dissipation is possible as long as N_1 is free to move, *i.e.* when it is in its immature or intermediates state. At the mature state, the N_1 node is bounded to the substrate to resist the contractile force. If the force on the node reaches the threshold F_{R1} then the node breaks and instantly dissipates the force (two occurrences for node 1 and node 5 in the figure). In both cases the sudden force increase in the branch is sufficient to reach the threshold force F_{th} on the N_0 node required for the cell to move (*i.e.* non-zero speed) just before the times 750s and 2000s. All other cases of cell displacements (*i.e.* non-zero speed) occurred when at least one branch becomes contractile to increase the resulting force on the N_0 node above the F_{th} threshold.

Figure 6: Upper graph: evolution of the force intensity in the different B_1 branches. The branches are displayed on 3 graphs to avoid overlapping of the co-existing branches. During the one-hour observation period 9 branches are observed with in average 3 co-existing branches. The colour code represents the maturation state of the branch: immature (green), intermediate (yellow), mature (red). Lower graph: evolution of the intensity of the resulting forces applied on the N_0 (first row) and N_1 nodes (rows 2 to 4). The N_1 nodes are displayed on 4 graphs to avoid overlapping of the co-existing nodes. During the one-hour observation period 9 N_1 nodes are observed. The colour code represents the maturation state of the N_1 node: immature (green), intermediate (yellow), mature (red). The horizontal grey dotted lines in each graphs represent the force thresholds $F_{R0} = F_{th}$ for N_0 to move and F_{R1} for N_1 to break.

3.2 Cell migration on a homogeneous substrate

To test the model we first perform cell migration simulations on a homogeneous substrate. Figure 7 (upper left graph) presents the superimpositions of 50 single cell trajectories recorded over 72 hours. The homogeneous distribution of the trajectories is coherent with a typical random migration behaviour, meaning that our model does not introduce any migration bias. We then tested the influence of the force attachment of the cell to the substrate. The cell attachment force corresponds to the threshold forces triplet (F_{th}, F_{R1}, F_{R2}) than can change depending on the biochemical nature of the substrate, *i.e.* on the cell matrix fibres composition, characterized by the amount of ligands and/or the strength of the adhesive bonds with which the cell can interact. To change the cell-substrate affinity, *i.e.* the cell attachment force, we introduce the parameter δ to modulate the force magnitude as $\delta \times (F_{th}, F_{R1}, F_{R2}) = (\delta F_{th}, \delta F_{R1}, \delta F_{R2})$. We then compare $\delta = 1$ which is the reference simulation with $\delta = 1.5$ which means a 50% increase of the attachment force. Figure 7 (upper right graph) shows that the cell exploration zone is significantly reduced while maintaining its random migration characteristic.

If δ is changed from 0.25 to 2.0, the average cell speed evolves with a bell shape (Fig.7, lower graph) which is in agreement with experimental facts [6]. For $\delta < 1$ the cell remains unable to move since the attachment force is too weak for the cell to take support on the substrate. The level of forces developed by the branches systematically break the adhesions that cannot strengthen and reach maturation to allow the cell to move. Once the attachment force is strong enough for $\delta > 1$ then the cell can move. For $\delta = 1.125$ the average cell speed reaches its maximum close to $8\mu m/h$, and decreases progressively for increasing values of δ. When the attachment force is higher, then the cell adhesions reach maturation however the forces developed in the branches are not high enough to reach the cell translocation threshold which limits the cell migration.

Since the level of force for cell translocation can only be reached once the N_1 adhesion is mature, we further tested the influence of the mature N_1 adhesion lifespan τ_m (Fig.7, lower graph). As expected, when the adhesion lifespan is shorter $(\tau_m/2 = 17min)$, there is a higher turnover of the adhesions which allows the cell to move more often, thus increasing the average migration speed. In the other hand when the lifespan is longer $(2 \times \tau_m = 70min)$, then the cell adhesion and its associated branch which does not reach the translocation threshold force remains stuck until the adhesion is released as it reaches its time limit. This is slowing down the cell migration speed. In the extreme case where the adhesion lifespan τ_m is infinite, the only way to break the adhesion is for the associated branch to reach the translocation threshold. The lack of adhesion turnover reduces drastically the average migration speed by a factor two

(the maximum speed is $4\mu m/h$), however the cell remains able to migrate.

Confrontation to experimental data

From a qualitative stand point, the bell shape relationship between the cell speed and cell attachment to the substrate is well described [6].

[9].

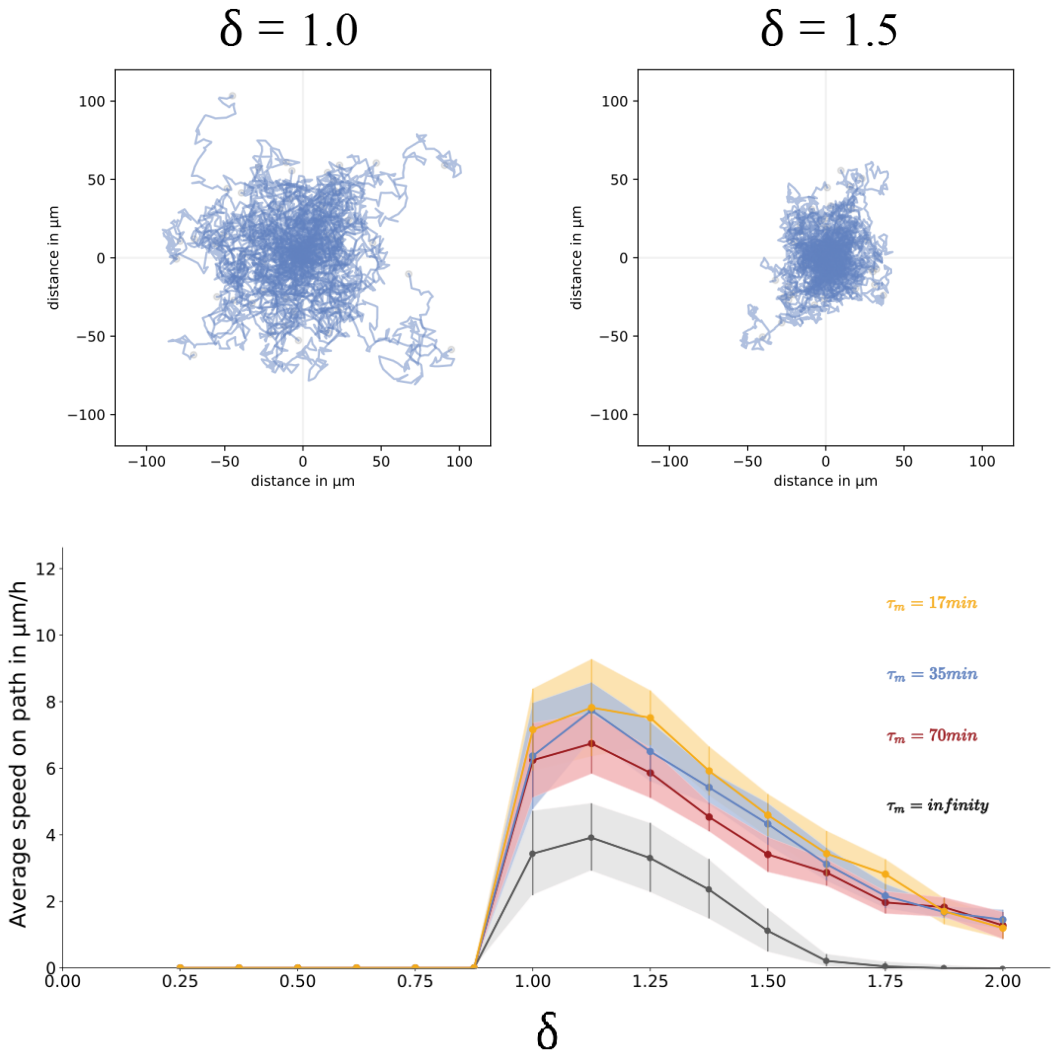

Figure 7: Upper graphs: Cell trajectories on a homogeneous substrate for two cell detachment conditions $\delta = 1.0$ and $\delta = 1.5$. Fifty trajectories of a single cell moving for 72 hours are superimposed in each graph. Lower graph: Average cells speed as a function of the parameter δ representing the cell detachment condition. Each point of the curves corresponds to 10 trajectories of a single cell moving for 12 hours. Each coloured curve corresponds to a different value for τ_m, the lifespan of mature N_1 nodes. $\tau_m = 35$ min is the reference simulation used in the two upper graphs.

3.3 Constrained cell migration on adhesive patterns

Engineered adhesive patterns, typically coated with fibronectin, are often used to constrain the cell shape in order to study the resulting cytoskeletal organization. They can also be used to investigate the factors influencing the cell displacements. Inspired by the study of Vecchio *et al.* [2], we challenged our cell model by constraining the cell migration on a stripe of adhesive triangular patterns. By varying pattern spacing, the aim is to determine if the pattern can favour a migration direction on our virtual cell. The triangular shape presents an adhesive asymmetry for the cell surface adherence between the left and the right side of the patterns. The question is *will the cell follow the arrows ?*

For the simulations, the nodes N_1 and N_2 can only form if in contact with the pattern. Each triangle of the pattern is $10\mu m$ high and $20\mu m$ long (Fig. 8). The gap distance between consecutive triangles is set for each simulations. It varies from -$12\mu m$ to $4\mu m$ with an increment of $4\mu m$ from one simulation to another. A negative value of the gap distance means that the triangles overlap with this length. We also considered a pattern of reference with no bias, corresponding to a continuous adhesive stripe.

Figure 8 (left) exhibits a sequence of cell movement and displacement on the adhesive pattern with a gap distance between consecutive triangles equals to zero. The cell forms branches that can reach the triangles on the left or on the right. However the inhibition condition for node and branch formation implemented in the model (see Fig. 2), limits the formation of a single branch per triangle (the triangle is not big enough to accommodate two N_1 nodes). As a consequence, the direction for the cell displacement is not the resultant of the force competition between left and right, since the forces tend to equilibrate with one branch on each side. On the other hand it mostly depends on the cell probability to form some adhesions, which is directly related to the differential length of the arcs corresponding to the intersection of the circle of radius l_{01} with the adhesive surface at each side of the cell. This is a strong difference with the experiments of Lo Vechhio et al. where the differential quantities between both sides of the cell is the adhesion area. Indeed the longer the arcs does not mean/correspond to the largest adhesion area.

To quantify the cell migration properties, Lo Vecchio et al. [2] proposed the calculation of a coefficient informing on the direction bias of the cell trajectory. This coefficient is calculated from the quantities N_+ and N_- that correspond respectively to the number of steps made by the cell in the positive direction (following the tips of the triangles) N_+

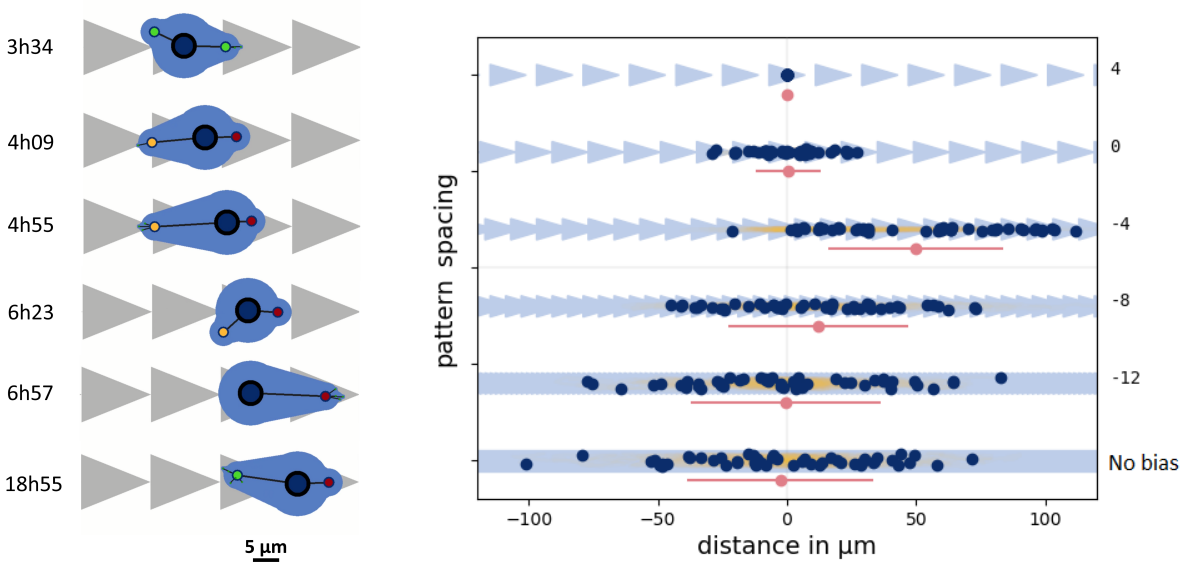

Figure 8: Left graph: cell displacement on triangular adhesive patterns. Right graph: each single cell was left to move on the pattern and its position after 72 hours is represented by a dark blue dot. The positions of 50 cells are displayed for each pattern spacing value. The average position and standard mean displacement are respectively represented by a red dot and line. The simulations are reproduced for different triangular pattern spacing from $4\mu m$ until there is a continuous adhesive strap (meaning no direction bias).

and in the negative direction (opposite direction) N_-.

$$p = \frac{N+ - N-}{N_+ + N_-} \tag{15}$$

4 Discussion

When the cells were allowed to migrate freely on a uniform substrate, as expected, no directional bias was observed. However, adhesion conditions clearly impacted cell movement. The model was be able to represent the experimentally observed bell shaped curve [6]. To do so, required matching the adhesion condition on N_1 nodes by adapting adapting the value of F_{R1}. The involvement of this parameter makes sens because it can be used to represent the strength of the adhesion between the cell and the substrate, which is changing experimental parameters such as fibronectin density and adhesion rupture force [6, 9]. However, to obtain the desired result, required a sufficiently long lifespan τ_m for mature N_1 nodes. These finding are coherent since the adhesion of slower moving cells are more stable and such behavior are found on rigid substrate or with increased fibronectin density. Thus changing a single mechanical

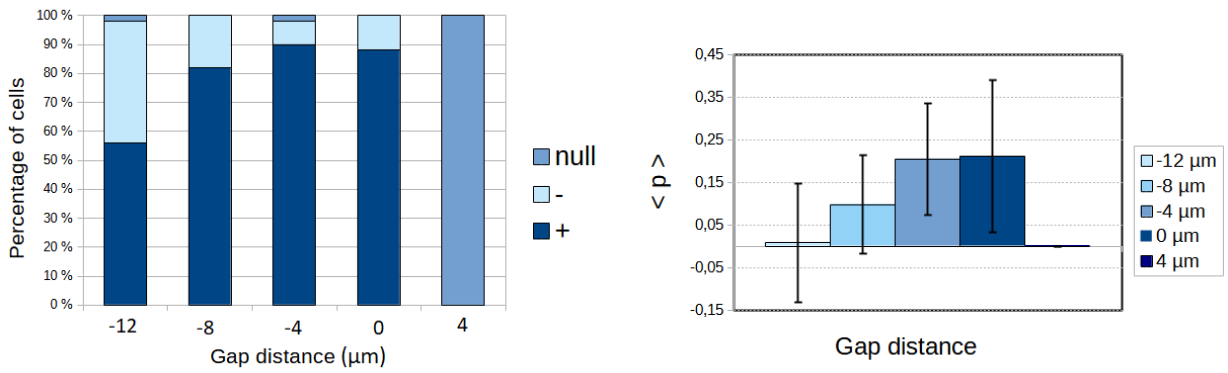

Figure 9: Left graph: percentage of cells ending their trajectories in the left side (-), right side (+) or same position (null) from their initial position, as a function of the gap distance. Right graph: average direction bias of the cell trajectories ($< p >$) as a function of the gap distance. Measurements in both graphs were made from 50 cells migrating for 48 hours.

parameter to represent the interaction with the substrate was enough to recreate the well documented behavior.

Vecchio et al. 2020 experimentally observed that, cells moved from on pattern to the next with a clear directional bias towards the right [2]. The model showed that it was able to generate a migration bias based on the spacing, height and length of the triangular pattern. To reproduce the observed behavior, we thus selected a parameter set that enabled cells to move from one pattern to the next and also showed a clear directional bias from left to right (fig8). Interestingly as the tips of the triangles became

However, while on the one hand, Vecchio et al. 2020, find that increasing spacing between the triangle patterns promoted directional bias to the right, on the other hand, in the model's case the bias was reduced ([2]). This can in part be explained by the fact that the model becomes less mobile as the inter-pattern distance increases. In the future, trying to improve the model on that count could be a valuable way to better understand the mechanism that allows cells to move from one pattern to the next.

Despite its relative simplicity, we were able to create a an agent based modeling scheme, that does not depend on a lattice. Moreover, the model takes into account both unicellular and extracellular mechanical forces, as well as substrate properties and reacts accordingly.

Performance wise, all computation was fast. 1h of single cell computation could be calculated in 0.2-20 seconds (without visualization) depending on settings. However, in the slowest simulations, the biggest performance hits

where caused by recording high amounts of data to disk, which could be optimized if needed. In addition, parallel optimization could be further implemented to process high cell count simulation in real time or even faster. The recorded computation speed suggests that the model could be implemented to study various multi-cellular phenomena such as morphogenesis, tissue patterning and angiogenesis, which was previously performed via a grid dependent modeling schemes [13, 18]. These simulation could therefore include a few hundred or even a few thousand cells, while delivering results within a reasonable time frame. In addition, the simplicity of the modeling paradigm makes it flexible enough to be adapted for various scenarios, which makes it a promising modeling framework for the future.

Acknowledgements

This work has been supported by the LabEx PERSYVAL-Lab (ANR-11-LABX-0025-01) funded by the French program Investissements d'avenir. It also received funding from PEPS CNRS - INSIS "La mécanique du futur" (2021).

Parameter	Description	Value	unit
ν_1	production rate of N_1	0.01	s^{-1}
ν_{2im}	production rate of N_2 from immature N_1	0.015	s^{-1}
ν_{2int}	production rate of N_2 from intermediate N_1	0.015	s^{-1}
ν_{2m}	production rate of N_2 from mature N_1	0.00001	s^{-1}
τ_t	duration of N_1 immature state	5	*min*
τ_{int}	lifespan of intermediate N_1	15	*min*
τ_m	lifespan of mature N_1	35	*min*
τ_2	lifespan of N_2	200	*s*
l_{10}	initial length of B_1	7	μm
l_{20}	initial length of B_2	4	μm
ε_m	maturation Cauchy strain of B_1	0.5	-
ε_{20}	initial Cauchy strain of B_2	0	-
κ_{10}	initial stiffness of B_1	0.1	$nN/\mu m$
κ_{11}	stiffness of B_1	3.5	$nN/\mu m$
κ_2	stiffness of B_2	12	$nN/\mu m$
α_0	friction coefficient of N_0	400	$nN \cdot s/\mu m$
α_{10}	initial friction coefficient of N_1	50	$nN \cdot s/\mu m$
α_{int}	friction coefficient of intermediate N_1	150	$nN \cdot s/\mu m$
α_m	friction coefficient of mature N_1	165	$nN \cdot s/\mu m$
α_2	friction coefficient of N_2	8	$nN \cdot s/\mu m$
γ_{max}	contractility of B_1	40	*nN*
F_γ	force constant	30	*nN*
F_{th}	Threshold force for N_0 displacement	30	*nN*
F_{R1}	Rupture force of N_1	34	*nN*
F_{R2}	Rupture force of N_2	17	*nN*
$\delta\theta_1$	inhibition angle for N_1	$\pi/2$	-
$\delta\theta_2$	apparition angle for N_2	$\pi/6$	-

Table 1: Model parameters

References

[1] David B. Brückner, Alexandra Fink, Christoph Schreiber, Peter J. F. Röttgermann, Joachim O. Rädler, and Chase P. Broedersz. Stochastic nonlinear dynamics of confined cell migration in two-state systems. *Nature Physics*, 15(6):595–601, June 2019.

[2] Simon Lo Vecchio, Raghavan Thiagarajan, David Caballero, Vincent Vigon, Laurent Navoret, Raphaël Voituriez, and Daniel Riveline. Collective Dynamics of Focal Adhesions Regulate Direction of Cell Motion. *Cell Systems*, 10(6):535–542.e4, June 2020.

[3] Roeland M.H. Merks, Sergey V. Brodsky, Michael S. Goligorksy, Stuart A. Newman, and James A. Glazier. Cell elongation is key to in silico replication of in vitro vasculogenesis and subsequent remodeling. *Developmental biology*, 289(1):44–54, January 2006.

[4] Graeme Donald Snooks. A general theory of complex living systems: Exploring the demand side of dynamics. *Complexity*, 13(6):12–20, July 2008.

[5] Adam Shellard and Roberto Mayor. Supracellular migration – beyond collective cell migration. *Journal of Cell Science*, 132(8), April 2019.

[6] Sean P. Palecek, Joseph C. Loftus, Mark H. Ginsberg, Douglas A. Lauffenburger, and Alan F. Horwitz. Integrin-ligand binding properties govern cell migration speed through cell-substratum adhesiveness. *Nature*, 385(6616):537–540, February 1997.

[7] Elisabeth G. Rens and Roeland M. H. Merks. Cell Shape and Durotaxis Follow from Mechanical Cell-Substrate Reciprocity and Focal Adhesion Dynamics: A Unifying Mathematical Model. *arXiv:1906.08962 [cond-mat, physics:physics, q-bio]*, June 2019.

[8] Kwang Hoon Song, Sung Jea Park, Dong Sung Kim, and Junsang Doh. Sinusoidal wavy surfaces for curvature-guided migration of T lymphocytes. *Biomaterials*, 51:151–160, May 2015.

[9] David Caballero, Raphaël Voituriez, and Daniel Riveline. Protrusion Fluctuations Direct Cell Motion. *Biophysical Journal*, 107(1):34–42, July 2014.

[10] David Caballero, Raphaël Voituriez, and Daniel Riveline. The cell ratchet: Interplay between efficient protrusions and adhesion determines cell motion. *Cell Adhesion & Migration*, 9(5):327–334, September 2015.

[11] Sonja E. M. Boas, Yi Jiang, Roeland M. H. Merks, Sotiris A. Prokopiou, and Elisabeth G. Rens. Cellular Potts Model: Applications to Vasculogenesis and Angiogenesis. In Pierre-Yves Louis and Francesca R. Nardi, editors, *Probabilistic Cellular Automata: Theory, Applications and Future Perspectives*, Emergence, Complexity and Computation, pages 279–310. Springer International Publishing, Cham, 2018.

[12] Margriet M. Palm, Marchien G. Dallinga, Erik van Dijk, Ingeborg Klaassen, Reinier O. Schlingemann, and Roeland M. H. Merks. Computational Screening of Tip and Stalk Cell Behavior Proposes a Role for Apelin Signaling in Sprout Progression. *PLOS ONE*, 11(11):e0159478, November 2016.

[13] A. Stéphanou, S. Le Floc'h, and A. Chauvière. A Hybrid Model to Test the Importance of Mechanical Cues Driving Cell Migration in Angiogenesis. *Mathematical Modelling of Natural Phenomena*, 10(1):142–166, 2015.

[14] Filippo Stefanoni, Maurizio Ventre, Francesco Mollica, and Paolo A. Netti. A numerical model for durotaxis. *Journal of Theoretical Biology*, 280(1):150–158, July 2011.

[15] Patrick Cañadas, Valerie M. Laurent, Christian Oddou, Daniel Isabey, and Sylvie Wendling. A cellular tensegrity model to analyse the structural viscoelasticity of the cytoskeleton. *Journal of Theoretical Biology*, 218(2):155–173, September 2002.

[16] Jean-Louis Milan, Sandrine Lavenus, Paul Pilet, Guy Louarn, Sylvie Wendling, Dominique Heymann, Pierre Layrolle, and Patrick Chabrand. Computational model combined with in vitro experiments to analyse mechanotransduction during mesenchymal stem cell adhesion. *European Cells & Materials*, 25:97–113, 2013.

[17] Jean-Louis Milan, Ian Manifacier, Kevin M. Beussman, Sangyoon J. Han, Nathan J. Sniadecki, Imad About, and Patrick Chabrand. In silico CDM model sheds light on force transmission in cell from focal adhesions to nucleus. *Journal of Biomechanics*, June 2016.

[18] M. Dorraki, A. Fouladzadeh, A. Allison, C. S. Bonder, and D. Abbott. Angiogenic Networks in Tumors—Insights via Mathematical Modeling. *IEEE Access*, 8:43215–43228, 2020.